Desalination and Water Treatment
www.deswater.com

doi: 10.5004/dwt.2019.23617

150 (2019) 1–8
May

Analysis of falling film flow and heat transfer on an elliptical tube

Bin Jiang[a,*], Manfeng Li[b], Qibin Tan[a], Anjie Hu[a]

[a]*School of Civil Engineering and Architecture, Southwest University of Science and Technology, Mianyang, 621010, China, emails: jiangbinustc@163.com (B. Jiang), qibintan@126.com (Q. Tan), anjie@swust.edu.cn (A. Hu)*
[b]*School of Environment and Municipal Engineering, North China University of Water Resource and Electric Power, Zhengzhou, 450046, China, email: limanfeng@nuwu.edu.cn*

Received 9 June 2018; Accepted 14 December 2018

ABSTRACT

Based on the volume of fluid algorithm and user-defined function, the flow and heat transfer of falling film on an elliptical transverse tube with different axis ratios was numerically studied. Simulation results are discussed based on the velocity, pressure, and temperature distribution of the liquid. According to the results, the liquid film pattern, heat and mass transfer of the liquid film are affected by the axis ratios: the liquid flow rate of the film outside the elliptical tube was faster compared with a circular tube; the simulated wall pressure gradually decreased along the flow direction and then rapidly recovered, and the position of the minimum pressure moved backwards with the increase of the axis ratio. Also, the distribution of local Nu along the wall was similar to the pressure distribution with the minimum value of $X = 0.90$. In general, the heat transfer of an elliptical tube performs best when the axis ratio is $e = 1.65$. The simulated Nu number distribution and film thickness were compared with published experimental data, which showed acceptable consistency.

Keywords: Falling film flow; Elliptical tube; Structure optimization; Heat and mass transfer

1. Introduction

Horizontal tube falling film evaporation has been widely used in many fields such as evaporation [1,2] and condensation [3], water desalination [4], refrigeration [5], and the petrochemical industry. Its advantages in heat transfer, such as high heat transfer efficiency, small heat transfer driving force, and excellent low temperature heat transfer performance have made it the main technology of low temperature multiple effect distillation [6]. This is a very promising seawater desalination method known for its high gained output ratio, convenience in power plant waste heat utilization, and low heat exchange resistance.

The flow and heat transfer characteristics of falling liquid film is influenced by various factors such as film flow rate, film temperature, film distributor height, and tube geometries. However, these parameters are quite difficult to measure with invasive measuring method, thus the non-invasive measuring method such as planar laser-induced fluorescence, particle image velocimetry, particle tracking velocimetry [7] and infrared thermography imaging [8] were employed in the previous research. The aforementioned factors adjust the effects of gravity, viscous shearing, surface tension and wall adhesion, and influence the film flow patterns and film stability, eventually affecting heat transfer performances. For example, the film surface of liquid film falling down a vertical plate with a non-uniform local heat source occurs a horizontal bump-shape. This bump-shape becomes unstable above a critical value of the imposed heat flux and deforms into vertical rivulets [9]. In the study by Schagen and Modigell [10], the calculated results, based on measured temperature profiles, show that enhancement of heat transfer in wavy film is dominated by the high frequent motion in the capillary wave region in front of the wave hump. In addition, for the purpose of providing a comprehensive account of the link between the interface height and film thickness and

* Corresponding author.

its fluctuations, the local and instantaneous flow rates are decomposed into steady and unsteady components in [7], the former represented by the product of the mean film height and mean bulk velocity and the latter by the covariance of the film-height and bulk-velocity fluctuations.

Heat transfer efficiency is the most important characteristics of falling film evaporation on a horizontal tube, and is highly dependent on the distribution of the liquid film [11]. When the liquid film falls on a horizontal tube, the heat is transferred from the tube wall, across the thin liquid layer, and then to the liquid gas interface, during which the heat transfer area and film thickness play important roles in thermal resistance.

The published works shows that with increases in film flow rate the average heat transfer coefficient of falling film evaporation decreases [12] or increases to a peak value then decreases [13], or first increases sharply then keeps almost constant [14,15]. The average heat transfer coefficient is independent of heat flux [16] in a non-boiling case. Lincong [17] proposed an egg-shaped horizontal tube. According to the numerical and experimental results, the egg-shaped tube can get a thinner liquid film and a better performance in heat transfer. Huijun and Jiong [18] numerically studied the falling film flow on a horizontal tube with a liquid discharge board, the results show that a liquid discharge board is beneficial to heat transfer. These works show that heat transfer can be enhanced by modifying the structure of the tube, nevertheless, the rule for the impact of the shape is still unclear, and needs to be further explored.

This work further discusses the influence of tube shape on liquid film distribution and heat transfer on a tube by taking an elliptical tube and numerically comparing it with a circular one. Different axis ratios were adopted in the work and their influences were studied in detail. The rest of the paper is arranged as follows: Section 1 presents the physical and numerical model; the simulation results are presented and discussed in Section 2; finally, a brief conclusion is made in Section 3

2. Numerical simulation method

In this work the mass, momentum, and temperature-governing equations were discretized using the second-order upwind scheme. The SIMPLE algorithm was applied for the pressure–velocity coupling. The governing equations were solved iteratively until they were convergent and the convergence criterion was 10^{-3} for all variables.

2.1. Geometry structure and grid division

The shape of the tube in the present work is an ellipse with a given outer perimeter of 59.69 mm (which can be considered as a deformed circular tube with diameter of 19.00 mm), as shown in Fig. 1. Distributors spray saturated water with temperature T_s onto the top of the horizontal tube, a water film is formed on the surface of the tube, it then accumulates at the bottom of the tube dropping onto the lower surface of the tube due to gravity and surface tension.

Fig. 2 shows the simulation domain and boundary conditions examined in the present work. In the simulation, the heat transfer inside the tube is neglected and thermal parameters along the surface of the tube are presumed constant. Since the flow outside the tube is symmetric, only half of the tube is simulated and symmetry boundary is applied on the symmetry axis. Other boundary conditions and liquid properties are given as follows: the velocity inlet width is set to 1 mm, and the liquid distribution height is set to 6 mm; a non-slip wall boundary is applied on the outer wall of the tube, and its temperature is set to be constant with 336 K; the temperature of the saturated water is set to 333 K, and its corresponding contact angle on the tube surface which is made of brass is set to 20° [19]. The detailed liquid parameters are shown in Table 1 and the simulation model settings are given in Table 2.

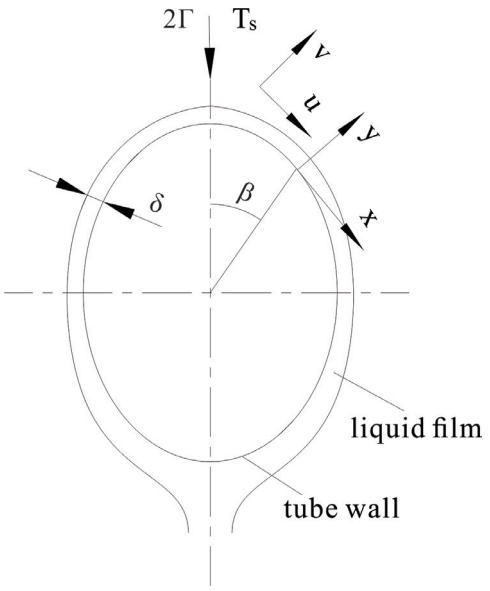

Fig. 1. Physical model of an elliptical tube falling film flow.

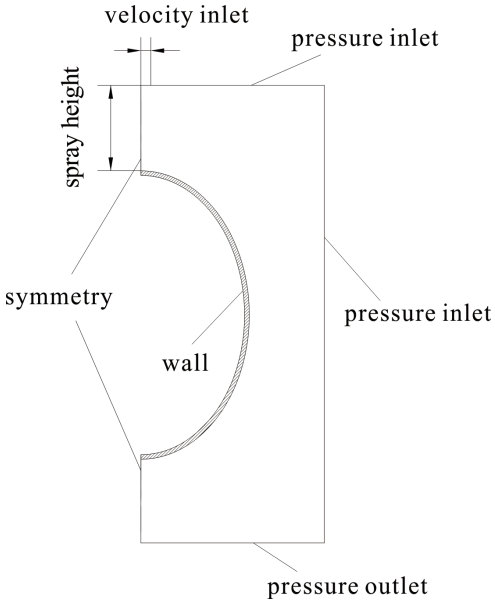

Fig. 2. Simulation domain and boundary conditions.

2.2. Axial ratios of elliptical tubes

In the present work, the elliptical tubes are introduced to improve the heat transfer of the liquid film. To investigate the influence of axial ratios on heat transfer efficiency and obtain the optimal ratio, different axial ratios (denoted by *e*) of elliptical tubes are applied. The axis ratio of the elliptical tube ranges from 1.0 to 5.0, as shown in Table 3. In the case of an axial ratio equal to 1, the shape of the tube is circular.

2.3. Numerical model

To eliminate interferences and better investigate the main factors that influence on the liquid flow, a simplified physical model is established by making the following assumptions: (1) the liquid is regarded as a continuous incompressible Newton fluid; (2) the temperature of the surface of the tube is set as constant; and (3) since the liquid evaporates little across one tube, phase transition is neglected in this case.

Based on these assumptions, the volume of fluid (VOF) model is used to capture the gas–liquid two phase interface. In this model, a component equation is considered, which can be written as follows:

Table 1
Properties of water at 333 K

Item	ρ/kg·m^{-3}	μ/kg·m^{-1}·s^{-1}	σ/N·m^{-1}
Saturated water	983.1	4.699×10^{-4}	0.06622
Saturated vapor	0.1302	1.042×10^{-5}	–

Table 2
Numerical simulation model settings

Setting	Models
Solver	Segregated unsteady
Viscous model	Laminar
Multiphase model	VOF
Pressure–velocity coupling scheme	PISO
Pressure	Body force weighted
Volume fraction	Geo-reconstruct
Surface tension force	CSF model

PISO, Pressure-implicit with splitting of operators.

Table 3
Tube sizes in present work

Serial number	Long axis, *a*/mm	Short axis, *b*/mm	Axial ratio, *e* = *a*/*b*	Perimeter, L/mm
Tube A	19.00	19.00	1.00	59.69
Tube B	21.60	16.21	1.33	59.69
Tube C	22.62	15.00	1.51	59.69
Tube D	23.30	14.13	1.65	59.69
Tube E	24.10	13.08	1.84	59.69
Tube F	25.20	11.50	2.19	59.69
Tube G	26.47	9.50	2.79	59.69
Tube H	28.27	6.00	4.71	59.69

$$\alpha_l + \alpha_\upsilon = 1 \tag{1}$$

where α_l, α_v are the volume fractions of saturated water and vapor, respectively.

The corresponding continuity equation for each phase is given by:

$$\frac{\partial \alpha_i}{\partial t} + \nabla \cdot \left(\vec{\upsilon}\alpha_i\right) = \frac{m_i}{\rho_i} \tag{2}$$

where α_i is the volume fraction of each phase, t is time (s), $\vec{\upsilon}$ is mixture velocity (m/s), m_i is the phase transition rates per unit (kg/(m^3·s)), and ρ_i is the density of each phase (kg/m^3).

The evaporation and condensation progress can be written as [20] follows:

$$m_\upsilon = 0.1 \cdot \alpha_\upsilon \rho_\upsilon \frac{T - T_s}{T_s}, \quad T \geq T_s \tag{3}$$

$$m_l = 0.1 \cdot \alpha_l \rho_l \frac{T - T_s}{T_s}, \quad T < T_s \tag{4}$$

where T_s is the saturation temperature (K); m_l and m_v are the phase transition rates per unit of saturated water and vapor, respectively; ρ_l and ρ_v are the density of saturated water and vapor, respectively.

The momentum equation is given by

$$\frac{\partial}{\partial t}\left(\rho\vec{\upsilon}\right) + \nabla\left(\rho\vec{\upsilon}\cdot\vec{\upsilon}\right) = -\nabla p + \nabla\left[\mu\left(\nabla\vec{\upsilon}\right)\right] + \rho\vec{g} + \vec{F}_{vol} \tag{5}$$

where ρ is the density (kg/m^3), p represents the pressure (Pa), μ is the dynamic viscosity (kg/(m·s)), g is the acceleration of gravity (m/s^2), and $\vec{F}_{vol}$ is the unit volume force (N/m^3).

The energy equation can be written as

$$\frac{\partial}{\partial t}\left(\rho h\right) + \nabla\left(\rho\vec{\upsilon}h\right) = -\nabla p + \nabla\left(\lambda\nabla T\right) + S_h \tag{6}$$

where h is the enthalpy per unit mass (J/kg), λ is the liquid thermal conductivity (W/(m·K)), and S_h is the energy source term (J/(m^3·s)).

Boundary conditions are expressed as:

Horizontal tube wall (y = 0)

$$u = v = 0, \; T = T_w \tag{7}$$

Interface of two phases (y = δ)

$$\frac{\partial u}{\partial y}\Big|_\delta = 0, \quad T = T_0 \tag{8}$$

where T_w is the wall temperature, and T_0 is the initial temperature of liquid entry. In this paper, $T_0 = T_s$.

To analyse the simulation results, several characteristic parameters are introduced in the present work. The Reynolds number (Re) which is given by

$$\mathrm{Re} = \frac{4\Gamma}{\mu} \tag{9}$$

where Γ is the unilateral saturated water flow rate.

Other characteristic parameters involved in the present work include: the dimensionless temperature, the dimensionless distance *X*, the dimensionless local film thickness η, the local Nusselt number Nu, the local Nusselt number is space-averaged value, the mean Nusselt number $\overline{\mathrm{Nu}}$ (the mean Nu number along semi-perimeter of elliptical tube), and local heat transfer coefficient h_w, W/(m²·K). These parameters are given by the following equations:

$$\Theta = \frac{T_w - T}{T_w - T_0} \tag{10}$$

$$X = \frac{l_x}{P} \tag{11}$$

$$\eta = \frac{y}{\delta} \tag{12}$$

$$\mathrm{Nu} = \left(\frac{\upsilon^2}{g}\right)^{1/3} \frac{h_w}{\lambda} \tag{13}$$

$$h_w = \frac{q_w}{T_w - T_0} \tag{14}$$

$$\overline{\mathrm{Nu}} = \frac{1}{P}\int_0^P \mathrm{Nu}\,\mathrm{d}x \tag{15}$$

where *P* is the semi-perimeter of the simulated tube surface, l_x is the distance between position *x* to the top of the tube surface, *y* is the distance between the wall and the given point, δ is the local film thickness (space-averaged), and *v* is the kinematic viscosity.

2.4. Grid independence verification

The thinner the liquid film, the better heat transfer performance. However, a continuous liquid film will not be formed if the water flow rate is too small. The local liquid film thickness with water flow rate Γ = 0.20 kg/(m·s), 0.35 kg/(m·s), 0.50 kg/(m·s) were calculated before the verification of grid independence, as shown in Fig. 3. The results show that the liquid film is thinner when Γ = 0.20 kg/(m·s). Thus, in the present study, the water flow rate is set to 0.20 kg/(m·s) (the corresponding Re is approximately 1,700).

To improve the accuracy of the simulation and reduce error, the grid independence is verified by simulating the liquid flow and heat transfer on a circular tube. The mesh quantities in the verification are chosen as 18,513, 32,753, and 46,437. In the simulation, the time step is set as 0.0001 s, and water flow rate is 0.20 kg/(m·s), the corresponding Re is approximately 1,700. Fig. 4 shows the simulation local liquid film thickness distribution of these three different meshes. As can be seen from this figure, the simulation results are very close to each other (the maximum deviation is about 0.74%) when the meshes mesh quantity are given as 32,753 and 46,437. However, the simulated thickness with mesh quantity of 18,513 is obviously different from the other cases. Fully considering calculation accuracy and efficiency, in this paper the mesh model with quantity of 32,753 was chosen for the following simulation. Specifically, the mesh sizes are set as flows: boundary layer encryption is applied along the tube surface and the mesh length is given as 0.05 mm, the mesh size in the simulation domain is 0.50 mm and generated with the quadrilateral mesh generation method.

3. Simulation results and discussion

3.1. Validation of simulation results

In order to verify the validity of the model, the simulation results are compared with published data. In the simulation, the shape of the tube is also set as circular. The simulated Nu number distribution was compared with published works in Fig. 5 [21,22]. It can be seen from the figure that the trends

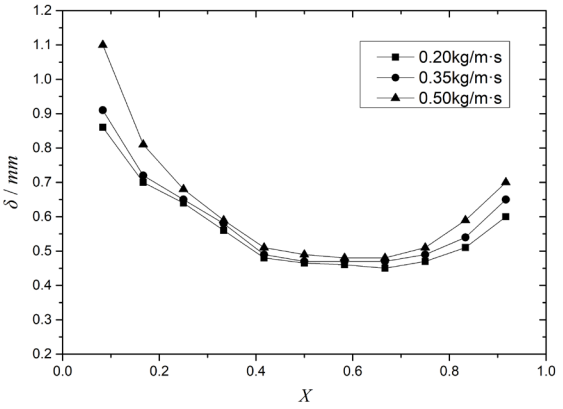

Fig. 3. Effect of spray density on local liquid film thickness.

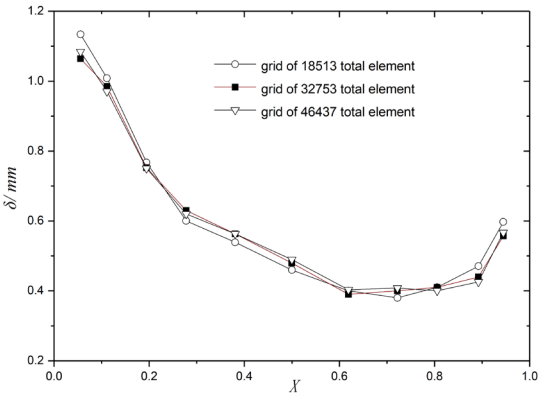

Fig. 4. Grid independence verification.

are very close to each other. The numerical calculation results are consistent with the experimental results, which verify the correctness of the numerical model established in this paper.

In addition, comparison of our numerical film thickness with the ones from the literature is conducted, as shown in Fig. 6. It can be seen that the present results agree well with the ones in the study by Hou et al. [23] but do not agree well with Nusselt's solution [24] due to the assumptions in Nusselt's analysis, as shown in Fig. 7.

3.2. Velocity and pressure distribution of liquid film

Higher film speeds tend to speed up liquid film renewal, which is conducive to the enhancement of heat transfer. Since the velocity distribution in the liquid film is directly affected by tube shape, to enhance the heat transfer on the tube the influence of the tube's shape on the liquid film velocity is numerically studied in this part.

Fig. 8 shows the space-averaged circumferential velocity profile when $\eta = 0.60$. It can be seen from the figure that with the increase of the axial ratio e, the velocity of the liquid also increases, however, the acceleration effect reduced along the circumferential direction of the tube. Specifically, for tubes A and B, the velocity profile first increases and then gradually falls due to the centrifugal force when $X > 0.80$. For tubes D, E, and, G, the liquid film velocity profile increases all along the tube, however, the increasing trend slows down when $X > 0.80$. These results show that the increase of e can reduce the flow resistance thus enhancing liquid renewal on the tube surface.

Besides the liquid film velocity, heat transfer is also influenced by the pressure distribution along the surface, since a lower pressure may eventually lead to the detachment of the film. Moreover, greater wall pressure is good for scouring the tube. Hence the pressure distribution is also simulated in the paper. Fig. 9 shows the relative pressure distribution along the surface. It can be seen from the figure that the pressure on the upper tube surface ($X < 0.50$) is positive due to the influence of gravity. However, the pressure becomes negative on the lower half of the tube, in this case the liquid film is attached on the wall by the effect of surface tension between the wall and the liquid. Finally, the pressure rebounds at the end of the tube due to the collision disturbance between the two symmetrical liquid films. The influence of axial ratio e can be also seen in this figure. With the increase of the axial ratio e, the pressure along the upper half of the tube decreases,

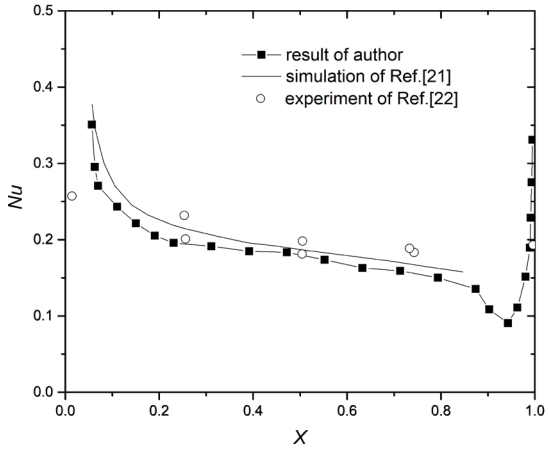

Fig. 5. Comparison of Nu number between the simulation results and published experimental results.

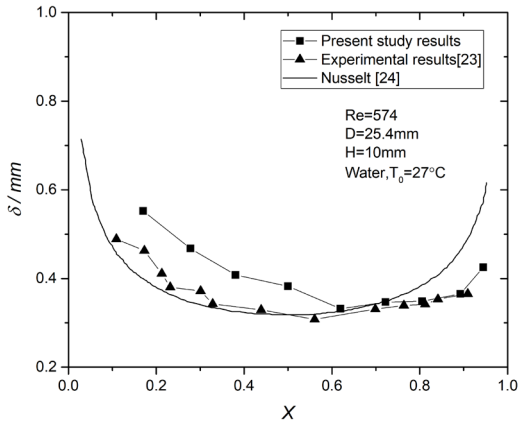

Fig. 7. Comparison of film thickness between present study and published experimental results.

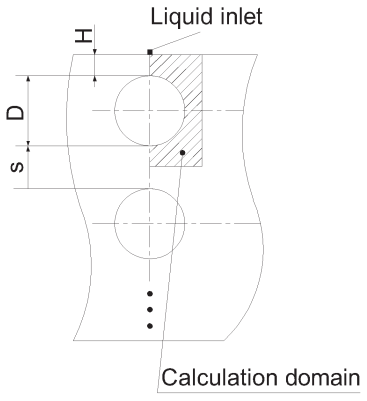

Fig. 6. Schematics of calculation domain in Ref. [23].

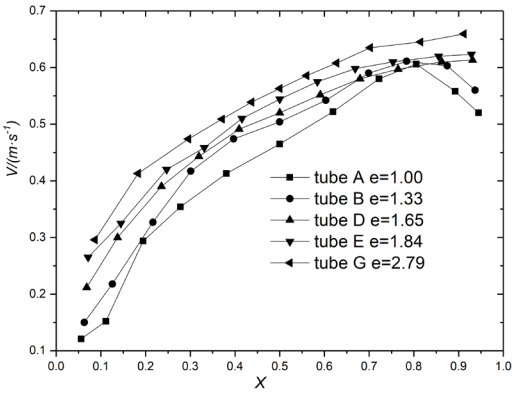

Fig. 8. Circumferential velocity profile when $\eta = 0.60$.

and the pressure along the lower half increases. Moreover, the pressure distribution with larger axial ratios is more uniform than the lower ratio cases. These results show that the liquid film can better attach to the tube surface when the axial ratio gets larger. Additionally, the minimum pressure is also influenced by the axial ratio and shifts around the position of $X = 0.90$. With an increase of the axis ratio, the position of the minimum pressure moves backwards, as shown in Fig. 9.

3.3. Heat transfer

Local heat transfer efficiency can be represented by the local Nusselt number. Fig. 10 shows the simulated distribution of the local Nusselt number along the tube. It can be seen from the figure that the Nu number distribution patterns are very similar for all tubes with different axial ratios. The Nu number is largest at the beginning of the tube where the liquid impacts on the surface. For the area of X ranging from 0.05 to 0.25, the Nu number quickly dropped along the flow direction as the flow film became steadier. For the area of X ranging from 0.25 to 0.80, the liquid flow is steadier and the declination of the Nu number is slower. The Nu number quickly drops again after $X > 0.80$, and reaches the minimum value around the area of $X = 0.90$. This is mainly caused by the negative pressure along the tube. The Nu number rises again at the end of the surface due to the collision disturbance between the two symmetrical liquid films.

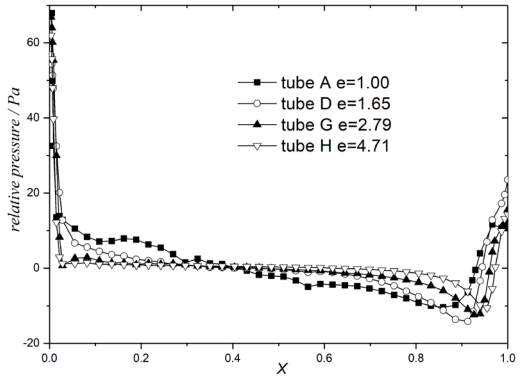

Fig. 9. Relative pressure distribution along the tube surface.

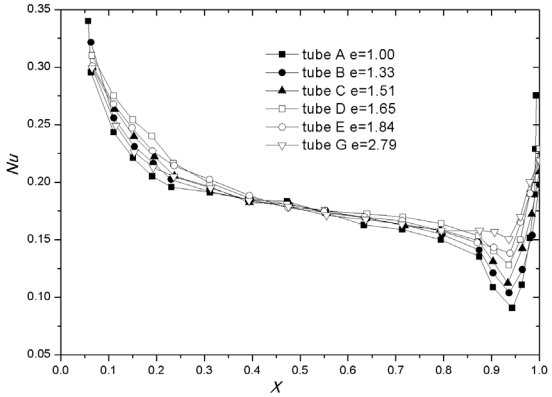

Fig. 10. Local Nu number along the circumferential wall.

To assess the heat transfer efficiency of tubes with different axial ratios, the average Nu number is also discussed in the present work. Fig. 11 shows the local Nu number for tubes with different axial ratios e. As we can see from the figure, the local Nu number increases first and then decreases as the axial ratio increases. According to the published work [25], the elliptic tube of $e = 1.50$ shows the best uniformity thin film among the four chosen elliptic tubes with axis ratios of 1.20, 1.50, 1.90, 2.1. Simulation results in the present work show that the Nu number reaches the highest value at $e = 1.65$ [25], which is very close to the result in the literature. The highest value of Nu number is 0.214, which is 6.5% higher compared with the circular tube. These results suggest that the elliptical tube is better in heat transfer enhancement.

Nevertheless, the conclusion that the Nu/HTC (heat transfer coefficient) becomes decoupled from the film thickness for Re > 1,000 was obtained on inclined heated foil (plane plate) [8] should be noticed. In the present manuscript, the conclusion was obtained from the research on horizontal tube. In the study by Lincong [17], the HTC on horizontal tube was experimentally tested for Re in the range 200–1,800. The results show that the Nu number increases monotonically as the Re number increases. However, the conclusion that the HTC/Nu becomes decoupled from the film thickness for Re > 1,000 was not reported.

3.4. Temperature distribution in the film

Heat transfer in the liquid film can be reflected by the temperature distribution in the liquid film. In general, the thinner the liquid film, the greater the temperature gradient, and the more conducive it is for heat transfer. Fig. 12 shows the non-dimensional temperature distribution at a given position for tubes with different axial ratios. It can be seen from the figure that the temperature gradient in the film of tube D is larger than tube A at the position of $X = 0.20$, mainly because of the drastic scouring on the top of tube D. Similar results can be found when $X = 0.40, 0.60, 0.80$. These results show that tube D is more suitable for heat transfer in these locations.

3.5. Heat transfer model analysis

To analyze falling film evaporation heat transfer, Cunfang et al. [26] divided the film into three zones (jet stagnation zone, thermal development zone, and fully development

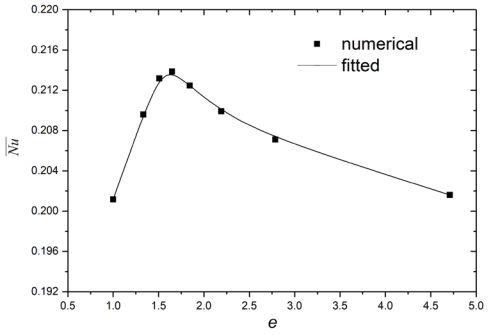

Fig. 11. Simulated Nu number with different axial ratios.

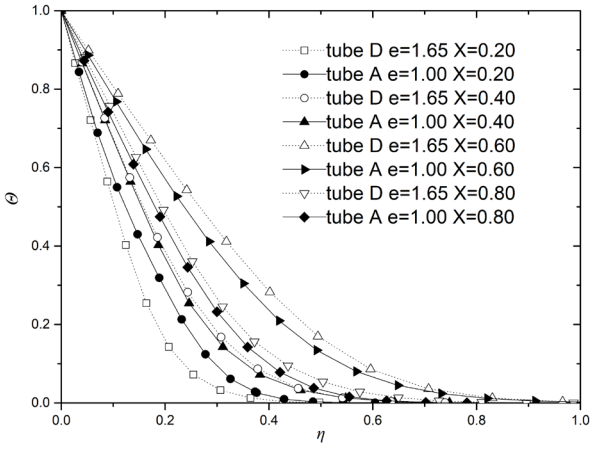

Fig. 12. Non-dimensional temperature comparison between elliptical and circular tubes under given relative coordinates.

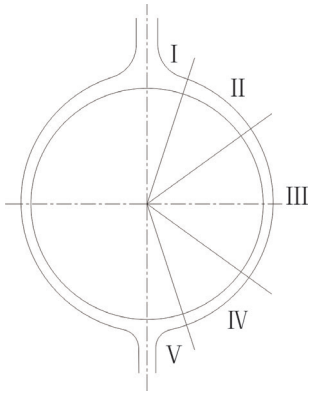

Fig. 13. Partition of heat transfer model.

zone) based on its heat transfer characteristics. However, according to the present work's simulation results of pressure distribution and Nu number distribution, these three zones cannot fully represent the characteristics of falling film evaporation heat transfer. Hence, a more detailed zoning is presented in the present work, as shown in Fig. 13.

The zoning method is given as follows:

- Zone I: Top impact zone ($X < 0.10$)
  Due to the impact of the falling liquid, the pressure and temperature difference gets to the maximum level at the beginning of this zone then rapidly reduces along the wall, and the heat transfer is also the strongest along the entire surface.
- Zone II: Heat exchange diffusion zone ($0.10 < X < 0.30$)
  In this zone, pressure and heat transfer decrease along the wall compared with zone I. The heat exchange capacity is still strong in this zone due to the large temperature difference and the increased flow speed.
- Zone III: Stable development zone ($0.30 < X < 0.70$)
  The temperature difference between the tube and the liquid gets smaller due to the increased temperature of the external liquid. The heat transfer is slightly weakened, and the external liquid flow rate increases rapidly. The heat transfer coefficient was kept high in the zone mainly because of the fast liquid film flow.
- Zone IV: Negative pressure zone (X about in the 0.70–0.90 range)
  The pressure continually decreases along the wall and becomes negative due to the negative pressure and small temperature difference. The heat transfer coefficient decreases gradually in the zone and the wall attaching ability of the flowing liquid becomes weak also because of the negative pressure along the wall.
- Zone V: Wake zone ($0.90 < X < 1.0$)
  In this zone, the flows compact from both sides and generate eddies beneath the tube. The heat transfer coefficient decreases quickly in the zone and reaches a minimum value due to the rapidly reduced pressure and small temperature difference. It then rises due to the strong turbulent flow generated by the impact of the flows.

4. Conclusions

In this paper, numerical simulation was adopted to study the falling film flow and heat transfer properties of an elliptical tube with different axis ratios by analyzing the obtained pressure distribution and liquid film velocity distribution conclusions can be drawn as follows:

(1) With an increase of the axial ratio e, the liquid film flow rate increases gradually. When $X = 0.80$, the acceleration tends to be 0, or even negative. Wall pressure reaches a minimum value in the vicinity of $X = 0.90$. With the increase of the axial ratio e, the minimum pressure position is moved backwards, and the pressure distribution is more uniform when $X = 0.10$–0.90.

(2) In addition to the zone affected by the impact of the liquid film on the top, the liquid film temperature gradient of the elliptical tube is greater than that of the circular tube, which is good for heat transfer.

(3) When $X = 0.90$ the wall pressure is minimal, the local Nu number is also at the minimum, and the pressure distribution is consistent with the Nu number distribution. The heat transfer performance of the falling film outside the elliptical tube is optimal when $e = 1.65$.

(4) According to this study a new zoning method of heat transfer in a horizontal tube has been put forward which can explain the heat transfer of an elliptical tube more clearly.

Acknowledgment

The present work was sponsored by the Science and Technology Project of the Ministry of Housing and Urban-Rural Development (2017-K8-025); the National Natural Science Foundation of China (51606159); and the Doctoral program of Southwest University of Science and Technology (11zx7106).

Symbols

e	—	Axial ratio
$\vec{F}_{vol}$	—	Unit volume force, N/m^3
g	—	Acceleration of gravity, m/s^2
h	—	Enthalpy, J/kg

h_w	—	Heat transfer coefficient, W/(m²·K)
l_x	—	Distance between the position x to the top of tube surface, m
m	—	Phase transition rates, kg/s
Nu	—	Nusselt number
p	—	Pressure, Pa
P	—	Semi-perimeter of tube surface, m
q_w	—	Wall heat flux, W/m²
Re	—	Reynolds number
S_h	—	Energy source term, J/(m³·s)
t	—	Time, s
T	—	Temperature, K
$\vec{v}$	—	Velocity, m/s
X	—	Dimensionless distance

Greek

a	—	Volume fractions
Γ	—	Unilateral saturated water flow rate, kg/(m·s)
δ	—	Film thickness, mm
η	—	Dimensionless film thickness
Θ	—	Dimensionless temperature
λ	—	Thermal conductivity, W/(m·K)
μ	—	Dynamic viscosity, kg/(m·s)
ρ	—	Density, kg/m³

Subscripts

i	—	Phase number
l	—	Liquid
s	—	Saturation
v	—	Vapor
w	—	Wall
0	—	Initial value

References

[1] C.Y. Zhao, P.H. Jin, W.T. Ji, W.Q. Tao, Heat transfer correlation of the falling film evaporation on a single horizontal smooth tube, Appl. Therm. Eng., 103 (2016) 177–186.

[2] C. Zhao, W. Ji, P. Jin, Y. Zhong, W. Tao, Hydrodynamic behaviors of the falling film flow on a horizontal tube and construction of new film thickness correlation, Int. J. Heat Mass Transf., 119 (2018) 564–576.

[3] Y.T. Kang, H. Hong, Y.S. Lee, Experimental correlation of falling film condensation on enhanced tubes with HFC134a; low-fin and Turbo-C tubes, Int. J. Refrig.-Rev. Int. Froid, 30 (2007) 805–811.

[4] H. Hou, Q. Bi, X. Zhang, Numerical simulation and performance analysis of horizontal-tube falling-film evaporators in seawater desalination, Int. Commun. Heat Mass Transf., 39 (2012) 46–51.

[5] G. Ji, J. Wu, Y. Chen, G. Ji, Asymmetric distribution of falling film solution flowing on hydrophilic horizontal round tube, Int. J. Refrig.-Rev. Int. Froid, 78 (2017) 83–92.

[6] F. Wunder, S. Enders, R. Semiat, Numerical simulation of heat transfer in a horizontal falling film evaporator of multiple-effect distillation, Desalination, 401 (2017) 206–229.

[7] A. Charogiannis, F. Denner, B.G.M.v. Wachem, S. Kalliadasis, C.N. Markides, Detailed hydrodynamic characterization of harmonically excited falling-film flows: A combined experimental and computational study, Phys. Rev. Fluids, 2 (2017) 014002.

[8] C.N. Markides, R. Mathie, A. Charogiannis, An experimental study of spatiotemporally resolved heat transfer in thin liquid-film flows falling over an inclined heated foil, Int. J. Heat Mass Transf., 93 (2016) 872–888.

[9] O.A. Kabov, B. Scheid, I.A. Sharina, J.C. Legros, Heat transfer and rivulet structures formation in a falling thin liquid film locally heated, Int. J. Therm. Sci., 41 (2002) 664–672.

[10] A. Schagen, M. Modigell, Local film thickness and temperature distribution measurement in wavy liquid films with a laser-induced luminescence technique, Exp. Fluids, 43 (2007) 209–221.

[11] Q. Qiu, C. Meng, S. Quan, W. Wang, 3-D simulation of flow behaviour and film distribution outside a horizontal tube, Int. J. Heat Mass Transf., 107 (2017) 1028–1034.

[12] W. Li, XiaoYuWu, Z. Luo, ShichuneYao, J. Xu, Heat transfer characteristics of falling film evaporation on horizontal tube arrays, Int. J. Heat Mass Transf., 54 (2011) 1986–1993.

[13] W. Li, X. Wu, Z. Luo, R.L. Webb, Falling water film evaporation on newly-designed enhanced tube bundles, Int. J. Heat Mass Transf., 54 (2011) 2990–2997.

[14] MarcelChristians, J. RichardThome, Falling film evaporation on enhanced tubes, part 1: Experimental results for pool boiling, onset-of-dryout and falling film evaporation, Int. J. Refrig.-Rev. Int. Froid, 35 (2012).

[15] M. Habert, J.R. Thome, Falling-Film Evaporation on Tube Bundle with Plain and Enhanced Tubes-Part I: Experimental Results, Exp. Heat Transf., 23 (2010) 259–280.

[16] Z. Liu, J. Yi, Enhanced evaporation heat transfer of water and R-11 falling film with the roll-worked enhanced tube bundle, Exp. Therm. Fluid Sci., 25 (2001) 447–455.

[17] L. Lincong, Analysis of Flow and Heat Transfer Enhancement and Experimental Research on Falling Film Evaporation on Horizontal Shaped Tubes, in, Shandong University, Jinan, P.R. China, 2014.

[18] L. Huijun, W. Jiong, Numerical simulation of falling film flow on horizontal circular tubes with drainage strips, Chin J. Power Eng., 36 (2016) 265–269.

[19] X.L. Lei, H.X. Li, Numerical Simulation of the Behavior of Falling Films on Horizontal Plain Tubes, in: AIP Conference Proceedings, Xi'an, China, 2010, pp. 998–1003.

[20] Z. Yang, X.F. Peng, P. Ye, Numerical and experimental investigation of two phase flow during boiling in a coiled tube, Int. J. Heat Mass Transf., 51 (2008) 1003–1016.

[21] D. Ouldhadda, A. Idrissi, M. Asbik, Heat transfer in non-Newtonian falling liquid film on a horizontal circular cylinder, Heat Mass Transfer, 38 (2002) 713–721.

[22] P.J.P. Liu, The Evaporating Falling-Film on Horizontal Tubes, in, University of Wisconsin-Masison, Masison, 1975.

[23] H. Hou, Q. Bi, H. Ma, G. Wu, Distribution characteristics of falling film thickness around a horizontal tube, Desalination, 285 (2012) 393–398.

[24] N. W, Die Oberflachenkondesation des Wasserdamffes the surface condensation of water, Zetrschr. Ver. Deutch. Ing., 60 (1916) 541–546.

[25] Q. Chunhua, F. Houjun, X. Yulei, Z. Heli, Numerical Simulation and Experimental Studies on Falling Film Outside Elliptical Tube: Experimental Study, Chem. Ind. Eng., 29 (2012) 43–47.

[26] L. Cunfang, Z. Mengzhu, G. Changming, Heat and Mass Transfer Model of a Single-tube Falling film Absorption Outside a Low Rib Horizontal Channel Tube and its Calculation, J. Therm. Energy Power Eng., China, 13 (1998) 351–354.